12th International Symposium on Turbulence and Shear Flow Phenomena (TSFP12)
Osaka, Japan (Online), July 19-22, 2022

A FLUID-STRUCTURE INTERACTION STUDY ON WAKE-INDUCED PENDULUM MOTION OF TANDEM CYLINDERS

Hyunjun Kim
Department of Naval Architecture and Ocean Eng.
Pusan National University
2, Busandaehakro 63beon-gil, Geumjeong-gu,
Busan 46241, Republic of Korea
junkim@pusan.ac.kr

Youngjin Jang
Hyundai Maritime Research Institute
Hyundai Heavy Industry
1000,Bangeojinsunhwan-doro,Dong-gu,
Ulsan 44032, Republic of Korea
andrewjang3774@hanmail.net

Inwon Lee
Department of Naval Architecture and Ocean Eng. Pusan National University
2, Busandaehakro 63beon-gil, Geumjeong-gu, Busan 46241, Republic of Korea
inwon@pusan.ac.kr

ABSTRACT

This paper presents an experimental investigation of the response characteristics of the pendulum motion of tandem cylinders undergoing wake-induced vibrations (WIV), which was first devised by Lee et al. (2021). In this pendulum system of tandem cylinders (PSTC), the downstream cylinder suspended from a pivot on the spanwise axis of the upstream cylinder oscillates in the circumferential direction in response to the incoming wake flow from the upstream cylinder. The governing parameters of the PSTC are the torsional spring stiffness, the cylinder spacing, and the moment of inertia of the system. The response characteristics for the WIV of the PSTC were measured experimentally by varying these main parameters. In addition, the relationship between two parameters, moment of inertia and torsional spring stiffness, was observed by changing individual values.

INTRODUCTION

When a cylinder is immersed in an incoming flow, vortices shed periodically from the cylinder exert an alternating lift force on the cylinder. If the cylinder is mounted on an elastic support, it undergoes periodic vibration, which is called "vortex-induced vibration (VIV)." If a cylinder is placed in front of a moving cylinder undergoing VIV at a distance close enough for the wakes from both cylinders to interact with each other, the motion of the downstream cylinder is affected by the wake generated by the upstream cylinder. This motion is called "wake-induced vibration (WIV)." This phenomenon can usually be realized by placing a stationary cylinder in front of the existing VIV system in a tandem arrangement. Many experimental studies have been attempted to observe and analyze this WIV phenomenon. Assi et al. (2010, 2013) conducted experiments with a staggered arrangement of two cylinders and found that WIV is influenced by the mean lift force by the wake within a specific linear range along the cross-flow direction, showing no resonance characteristics of VIV. This linearity of mean lift force along the cross-flow direction is called "wake stiffness," and was proven in the WIV experimental setup without a spring. For tandem cylinders with different diameters, Assi (2014) showed that displacement in the cross-flow direction of the downstream cylinder became smaller as the downstream cylinder becomes larger.

In a recent study by the authors (Lee et al. 2021), a novel swinging WIV was devised and analyzed numerically through large eddy simulation (LES). While the existing WIV system consists of a tandem arrangement of cylinders in translational motion, the present swinging WIV system, called a "pendulum system of tandem cylinders (PSTC)," exhibits an oscillatory, revolving motion of the downstream cylinder pivoted to the upstream cylinder. In a numerical simulation by Lee et al. (2021), the present PSTC was observed to have higher energy converting capability compared to that of the conventional "translational system of tandem cylinders (TSTC)." The higher efficiency of the PSTC was attributed to an increase in the oscillation frequency due to the additional restoring force contribution from drag force.

In this study, the response characteristics of the PSTC are investigated experimentally in detail by varying parameters such as torsional spring stiffness, the weight of the downstream cylinder, and the distance between the cylinders. To assess the mechanical energy conversion performance of the present PSTC, the mechanical power was calculated based on the measured torque and the angular velocity. This power can be utilized as a comprehensive measure to evaluate the spectral characteristics of torque and angular displacement of the present pendulum oscillation system.

EXPERIMENTAL SETUP

The experimental apparatus used in this study is shown in Fig. 1. It was mounted on the measurement rail of the carriage of a towing tank in Pusan National University. The towing tank dimensions are 100 m (length) × 8 m (width) × 3.5 m (depth). Uniform inflow to the PSTC was generated by moving the carriage. In this study, the carriage speed was limited to 4 m/s due to the excessive VIV of the fixed upstream cylinder beyond this speed.

The rotating pipe pivots on the fixed inner cylinder, which extends downward to form the upstream cylinder of the PSTC. The downstream cylinder is supported at both ends by connecting plates that connect the downstream cylinder to the rotating pipe. Thus, the pipe rotates in accordance with the swinging motion of the downstream cylinder, whose angular displacement is measured by a potentiometer. In order to amplify the potentiometer response, multiplying gear with a gear ratio of 5 is installed between the rotating pipe and the potentiometer.

The external hydrodynamic torque acting on the rotating pipe is measured by the dynamometer. The connecting plates have four holes, by which the cylinder spacing S can be varied as $S/D = 2, 3, 4, 5$.

CHARACTERISTICS OF WIV RESPONSE

The response characteristics of the present pendulum system (PSTC) depend on three main parameters: the cylinder spacing S, the moment of inertia I and the natural frequency of the rotating system f_0. In this study, a total of 14 cases were selected to investigate the effect of the three parameters on the pendulum motion response, as shown in Table 1. Each case name consists of five strings (case identifiers), which signify the approximate values of spring stiffness (KXX), nondimensional cylinder spacing S/D (SX), mass of the downstream cylinder (MXX), moment of inertia (IXX) and natural frequency (FXX).

Table 1. List of test cases

No.	Case name
1	K00-S4-M047-I035-F00
2	K00-S4-M230-I108-F00
3	K10-S4-M047-I035-F27
4	K10-S4-M230-I108-F15
5	K21-S4-M047-I035-F39
6	K26-S4-M047-I035-F43
7	K26-S4-M230-I108-F24
8	K29-S2-M290-I045-F40
9	K29-S3-M130-I045-F40
10	K29-S4-M073-I045-F40
11	K29-S5-M047-I045-F40
12	K40-S4-M047-I035-F54
13	K40-S4-M117-I063-F40
14	K40-S4-M230-I108-F31

The 14 cases can be subdivided into four groups. In the first group listed in Table 2, the nondimensional cylinder spacing S/D is varied. Here, the mass of the downstream cylinder for each case was chosen such that the moment of inertia I remains unchanged in spite of the varying cylinder spacings. In addition, the spring stiffness k was kept constant, thereby making the natural frequency constant. In this manner, the effect of S/D on the WIV response was able to be isolated. Test cases listed in Table 3 correspond to the variation of the natural frequency f_0 by means of changing spring stiffness k.

Assi et al. (2013) showed that the wake behind the upstream cylinder can operate as a stiffness element and called this "wake stiffness" in the WIV response. Here, the word "stiffness" is used because the mean lift changes linearly with the position of the downstream cylinder in the cross-flow direction in the wake of the upstream cylinder. With the wake stiffness being dominant, the amplitude of the lift force and consequently the response of the downstream cylinder becomes linearly proportional to the reduced velocity. Assi et al. (2013) noted that the WIV response characteristics can be divided into three regions, the VIV response region, the wake stiffness region, and the pure wake region. It is noteworthy that the swinging WIV response for the present PSTC shows similar behaviors as those observed for the translational WIV of Assi et al. (2013).

Table 2. Variation of the cylinder spacing

No.	Case name	k [N·m/rad]	S/D	M [kg]	I [kg·m^2]	f_0 [Hz]	ζ
8	K29-S2-M290-I045-F40	0.293	2	2.90	0.045	0.404	0.0260
9	K29-S3-M130-I045-F40		3	1.30			0.0321
10	K29-S4-M073-I045-F40		4	0.73			0.0330
11	K29-S5-M047-I045-F40		5	0.47			0.0385

Table 3. Variation of spring stiffness

No.	Case name	k [N·m/rad]	S/D	M [kg]	I [kg·m^2]	f_0 [Hz]	ζ
2	K00-S4-M230-I108-F00	0.000	4	2.30	0.108	0.000	0.0070
4	K10-S4-M230-I108-F15	0.0976				0.151	0.0077
7	K26-S4-M230-I108-F24	0.2553				0.245	0.0062
14	K40-S4-M230-I108-F31	0.4022				0.307	0.0077

Figure 2 presents 2D contour plots of four major WIV response variables, i.e., the root mean square of angular displacement $\hat{\theta}$, dominant frequency f_θ, torque coefficient C_τ and power P as a function of Reynolds number Re and the natural frequency f_0. Here, the dominant frequency is defined as the peak frequency where the power spectrum of angular displacement becomes maximum. The torque coefficient C_τ and the power P can be calculated as follows:

$$C_\tau = \frac{\hat{\tau}}{0.5\rho V^2 D^3} \quad (1)$$

$$P = \frac{1}{t_2 - t_1}\int_{t_1}^{t_2} |\tau\dot{\theta}| dt \quad (2)$$

Here, $\hat{\tau}$ represents the root mean square of torque fluctuations.

In Fig. 2 (a), it is observed that angular displacement $\hat{\theta}$ becomes larger in the lower right corner of the domain, i.e., a high Reynolds number and low natural frequency. On the other hand, the dominant frequency f_θ is maximized for high Re and high f_0, as in Fig. 2 (b). Although both $\hat{\theta}$ and f_θ increase with increasing Re in general, the tendency of increase appears differently for each natural frequency f_0 case. For instance, for the low natural frequency region ($f_0 \leq 0.1Hz$), the increase in $\hat{\theta}$ with increasing Re occurs rather abruptly for $Re \geq 1.2 \times 10^4$, while the increase in $\hat{\theta}$ appears more gradually for higher natural frequencies, as shown in Fig. 2 (a). In Fig. 2 (b), a low frequency domain with $f_\theta \leq 0.45Hz$ for low natural frequencies is marked.

This implies that the frequency of WIV does not necessarily follow monotonically increasing trend.

In summary, it is observed that the swinging WIV response depends not only on the natural frequency f_0 but also on other parameters such as the moment of inertia and Reynolds number in rather complicated manners.

Effect of nondimensional cylinder spacing *S/D* with constant natural frequency

Figure 3 plots the RMS angular displacement $\hat{\theta}$, dominant frequency f_θ, torque coefficient C_τ and power P as a function of Reynolds number. It is worthwhile to mention that this power is not the actual power harnessed from the generator, but the mechanically converted energy from the hydrokinetic energy. For $S/D = 2$, the cylinder spacing is too close for the gap flow to develop. Thus, case S2 shows a much smaller motion response than other cases do. The RMS angular displacement $\hat{\theta}$ become largest for cases S3 and S4. While S3 and S4 have almost the same magnitude of RMS angular displacement, S4 is found to have a slightly higher frequency than S3. As a result, case S4 shows the largest power, as in Fig. 3 (d). For the sake of brevity, the nondimensional spacing is fixed as $S/D = 4$ in the following parametric investigations.

Effect of spring stiffness with high moment of inertia

In this group of cases, the moment of inertia was increased about three times ($I = 0.108\ \mathrm{kg \cdot m^2}$) and other parameters were kept the same as the previous group. The results are plotted in Fig. 4. As seen, a noticeable change was found in $\hat{\theta}$ with respect to Re. As seen in Fig. 4 (a), the motion response $\hat{\theta}$ for the case without a spring (K00 case) becomes largest for $Re \geq 1.5 \times 10^4$, which is in contrast to the smallest response for $Re \leq 1.1 \times 10^4$. On the other hand, the case with highest spring stiffness (K40 case) shows a significantly smaller response $\hat{\theta}$ for $Re \geq 1.2 \times 10^4$. In Fig. 14 (b), the dominant frequency f_θ follows the constant Strouhal number line $St = fD/U = 0.2$ in the Reynolds number up to $Re = 0.6 \times 10^4$. Beyond this, the dominant frequency becomes larger with increasing stiffness, which follows the same trends as the natural frequency $f_0 = \frac{1}{2\pi}\sqrt{k/I}$. Similar to before, the power becomes smallest for the highest stiffness case.

FREQUENCY SIGNATURES OF DOWNSTREAM CYLINDER

For the first group of test conditions explained above, the normalized power spectral density (PSD) for the angular displacement θ and the torque τ acting on the downstream cylinder are plotted in Fig. 5. Here, the PSD is defined as the Fourier transform of autocorrelation functions of each quantity (angular displacement and torque) measured at each velocity as follows:

$$S_{xx}(f) = \int_{-\infty}^{\infty} R_{xx}(t) e^{-j2\pi f t} dt. \qquad (3)$$

Here, the subscript x denotes the quantity under consideration, which corresponds to either the angular displacement θ or the torque τ. The normalized PSD is then calculated by dividing $S_{xx}(f)$ by maximum value $S_{xx,max}$; therefore, its value ranges from 0 to 1. Such normalized PSDs at each velocity are gathered together to represent the variation of dominant frequency components in 2D velocity-frequency space with the dark grey cells representing dominant frequency component. It is worthwhile to mention that the frequency axis for the 2D contours is defined differently depending on the existence of a torsional spring. In every plot, a constant Strouhal number line $St = fD/U = 0.2$ is drawn to visualize the lock-in region in the 2D velocity-frequency space.References to original sources for cited material should be listed together at the end of the paper; footnotes should not be used for this purpose.

Figure 5 demonstrates the frequency signature plots for the first group of test cases involved in the variation of cylinder spacing S. For the smallest spacing $S/D = 2$ in Fig. 5 (a), the major frequency component for θ is found along the horizontal axis, i.e., $f/f_0 = 0$. In other words, the angular displacement for this case hardly presents periodic oscillation, which is in accordance with the noticeably small values of the RMS angular displacement $\hat{\theta}$ in Fig. 5 (a). In addition, the θ–contour on the left and the τ–contour on the right are poorly correlated, which accounts for the near-zero power for this case shown in Fig. 5 (d). For the case of $S/D = 3$ in Fig. 5 (b), it is found that frequency components are spread in a rather wide frequency range. This is in contrast to the narrow, sharp branches observed for the cases $S/D = 4$ in Fig. 5 (c) and $S/D = 5$ in Fig. 5 (d). In all cases in this group, the major branches do not follow the constant Strouhal number line $St = 0.2$.

CONCLUSIONS

In this study, the swinging WIV response characteristics of the pendulum system of tandem cylinders (PSTC) devised by Lee et al. (2021) were investigated with a series of towing tank measurements. The aim of the present study was to analyze the effect of the system parameters on the WIV response characteristics. It is observed that the RMS angular displacement $\hat{\theta}$ becomes smaller and the dominant frequency f_θ becomes larger with increasing spring stiffness, and this characteristic becomes clearer as the moment of inertia becomes large. This is attributable to the smaller damping ratio associated with the large moment of inertia cases. It can be concluded that the effect of the moment of inertia is larger than that of the spring stiffness.

ACKNOWLDEGEMENT

This work was supported by the National Research Foundation of Korea (NRF) grant funded by the Ministry of Science and ICT of Korea (No. 2022R1A2C2010821), to which deep gratitude is expressed.

REFERENCES

Assi, G. R. S., Bearman, P. W., Carmo, B. S., Meneghini, J. R., Sherwin, S. J., Willden, R. H. J., 2013, "The role of wake stiffness on the wake-induced vibration of the downstream cylinder of a tandem pair," *Journal of Fluid Mechanics*, Vol. 718, pp. 210-245.

Assi, G. R. S., 2014. "Wake-induced vibration of tandem cylinders of different diameters," *Journal of Fluids and Structures*, Vol. 50, pp. 329-339.

Lee, C. M., Paik, K-J., Kim, E. S., Lee, I., 2021, "A fluid–structure interaction simulation on the wake-induced vibration of tandem cylinders with pivoted rotational motion, " *Physics of Fluids*, Vol. 33, 045107

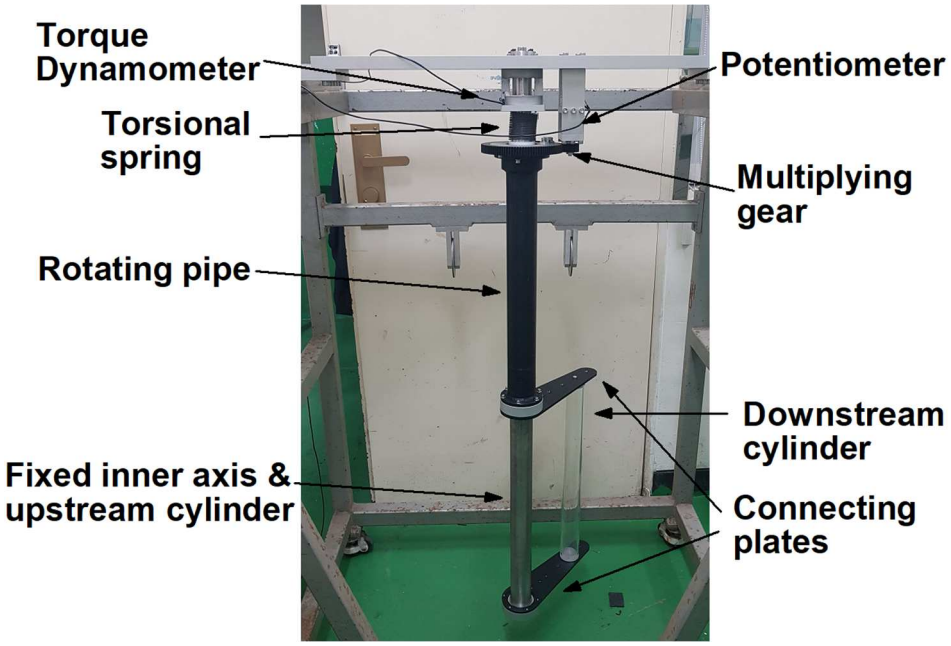

Figure 1. The PSTC apparatus

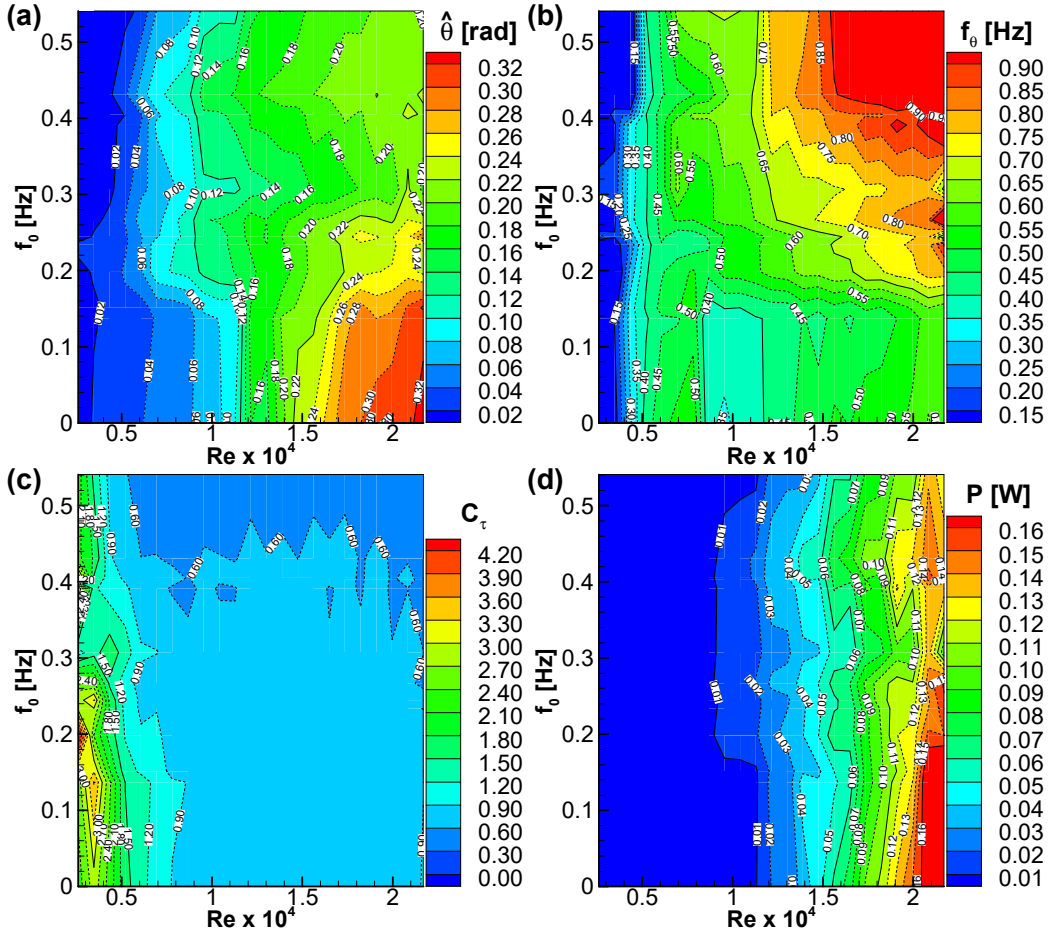

Figure 2. Contour plots of swinging WIV response with respect to Re and natural frequency f_0: (a) RMS angular displacement $\hat{\theta}$, (b) dominant frequency f_θ, (c) torque coefficient C_τ, (d) power P

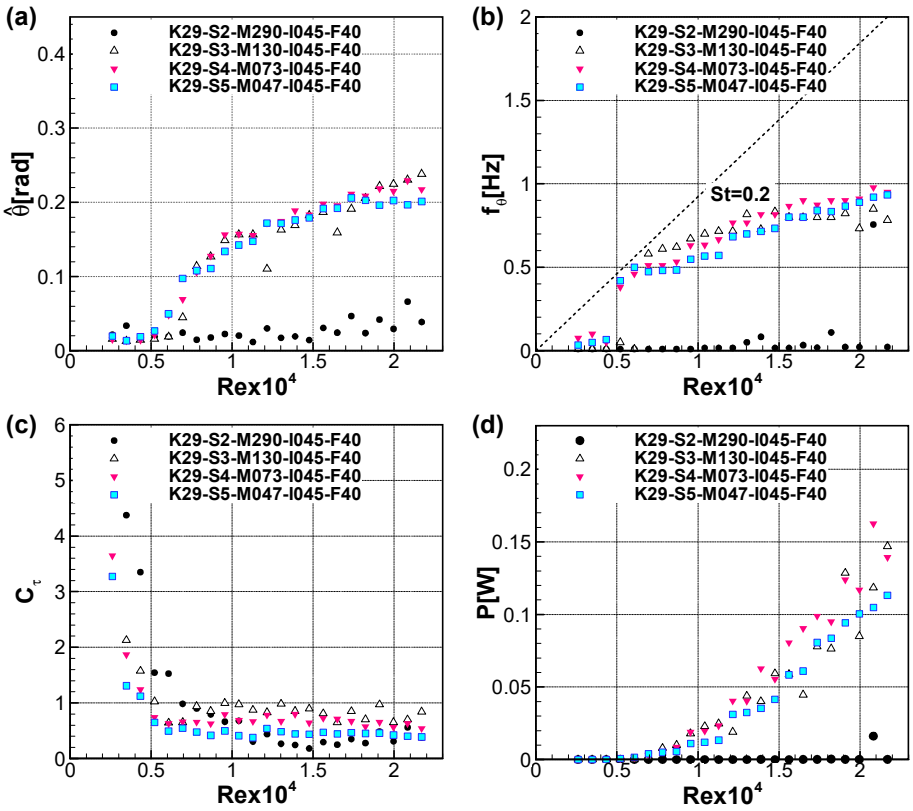

Figure 3. WIV response for varying cylinder spacings with constant natural frequency: (a) RMS angular displacement $\hat{\theta}$, (b) dominant frequency f_θ, (c) torque coefficient C_τ, (d) power P

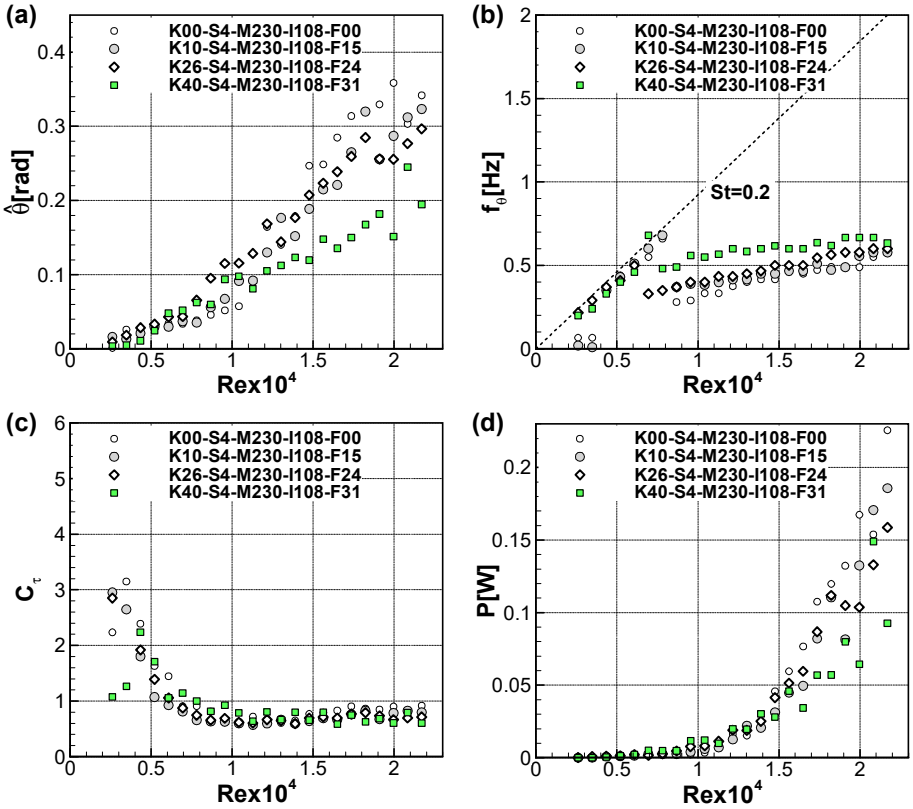

Figure 4. WIV response for varying spring stiffness with large moment of inertia ($I = 0.108\ \mathrm{kg \cdot m^2}$): (a) RMS angular displacement $\hat{\theta}$, (b) dominant frequency f_θ, (c) torque coefficient C_τ, (d) power P

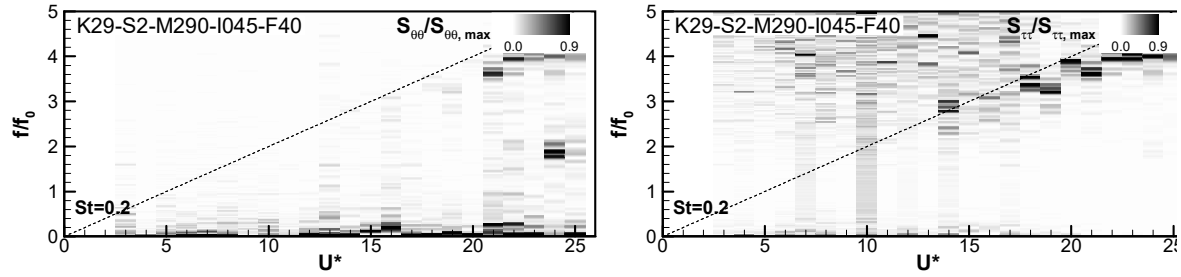

(a) K29-S2-M290-I045-F40

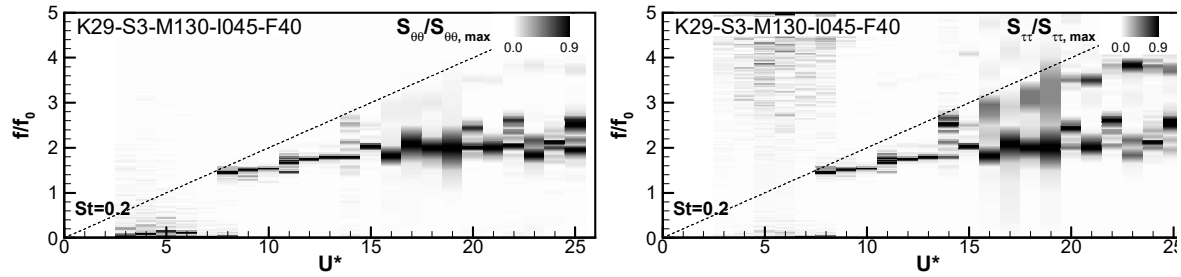

(b) K29-S3- M130-I045-F40

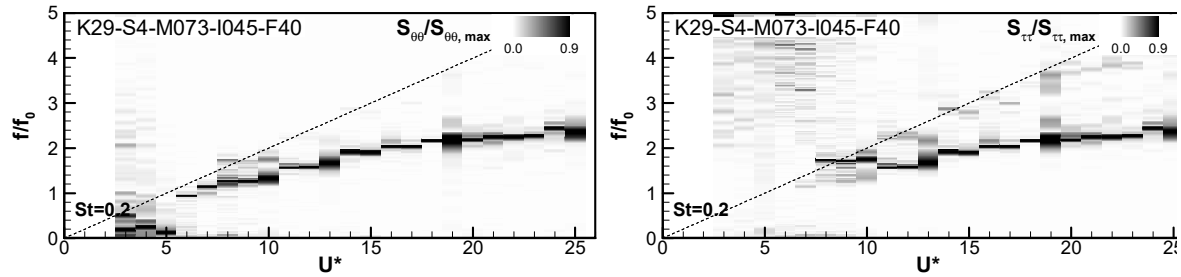

(c) K29-S4-M073-I045-F40

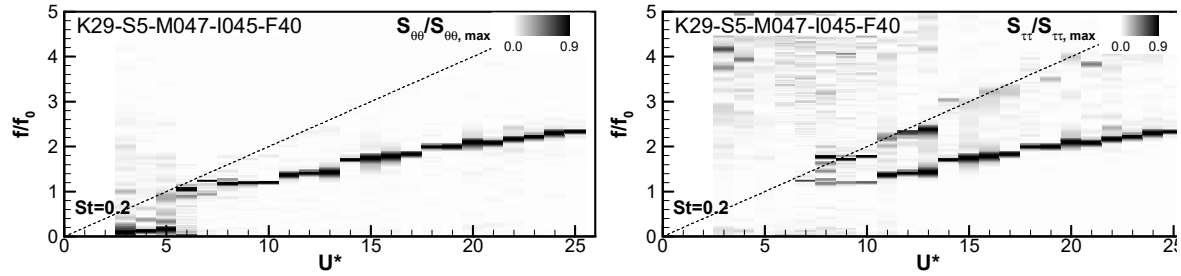

(d) K29-S5-M047-I045-F40

Figure 5. Normalized power spectral density (PSD) of the angular displacement θ and torque τ for various cylinder spacings S